WP2 (Objectives 1-3): Develop a comprehensive genome-scale mathematical model of the BMMSC-myeloma cell metabolic network.

Understanding the metabolic interactions within a multicellular context requires a fundamental and exhaustive analysis. Whilst we have substantial experience in interpreting the datasets of mass isotopomers describing the incorporation of ^{13}C atoms into diverse cellular metabolites, a bottleneck arises when a co-culture experimental setup is utilised due to its complexity increasing several-fold. As a consequence, full knowledge of the system is difficult, if not impossible, to be attained. To resolve this bottleneck, we adopt the use of an *"in-silico"* comprehensive modelling approach.

To this end, we have devised a **preliminary** multicellular metabolic network employing the computational **flux balance analysis** (**FBA**) framework - **a genome-scale method** for simulating metabolic networks in cells.

Briefly, this mathematical approach requires a stoichiometric matrix (S), which represents all the reactions and metabolites of interest. The matrix (S) is constructed under the assumption that the system is at a quasi-steady state (i.e., $S \cdot v = 0$); where v is a flux distribution vector. Flux capacity and directionality constraints are included by defining upper and lower bounds ($v_{min} < v < v_{max}$) of individual reactions. Through conical optimisation routines (e.g., linear programming), and establishing biologically relevant objectives (such as myeloma proliferation via biomass growth). The result is a continuous flux distribution space (a set of physiologically viable solutions known as the ***"flux hyper-cone"***) without requiring previous knowledge of any transient behaviours or metabolite concentrations. Here, a unique solution (guided by experimental data) ought to be found. This "unique" solution directly translates into **qualitatively testable predictions**.

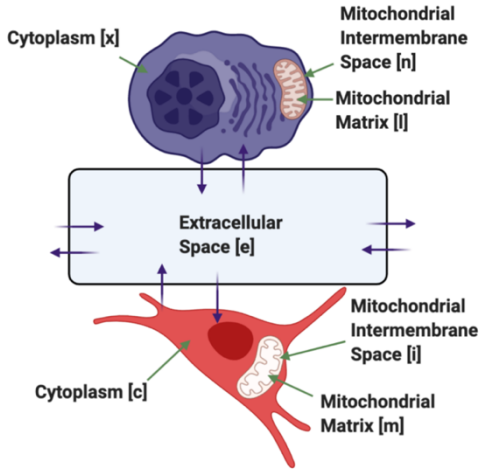

Fig. 1: A. *Schematic of the multicellular modelling approach. The BMMSC is depicted in red, where the flow of metabolites (represented in lilac arrows) is bidirectional, always from and towards the extracellular space. From here, they are either directed towards the myeloma cell (depicted in dark purple) or in/out the microenvironment niche. For differentiating cell specific models, all reactions were annotated with [c], [m], [i], [x], [l], [n], and [e] for the distinct compartments respectively.*

Our model consists of a multi-compartmental (i.e., interstitium, cytoplasm, and mitochondrion) and multicellular architecture, where the relevant metabolite cross-feed occurs via a reaction network spanning a BMMSC and a myeloma cell embedded in a hypoxic microenvironment niche - with an oxygen tension ($\mathbf{P_x O_2}$) of approximately 2% (**Fig. 1**). The setup aims to reproduce the physiological conditions in which these cells are localised (i.e. the bone marrow). Each cell is equipped with the ability for its metabolites to exit or enter, via relevant plasma membrane molecular machinery bordering an extracellular compartment, which complies with several critical physiological functions such as metabolite exchange, pH regulation, and the ability to rid any excess metabolites like urea or lactate, amongst others (**Fig. 1**).

It is important to remark that our preliminary model is exclusively **based on first principles (i.e. mass conservation and compartmental electroneutrality) and the stoichiometries of the metabolic reactions that take place in each cell.** Thus, all inputs and outputs are relative rather than absolute. Taking this approach implies that any prediction of the model is qualitative, not quantitative. Additionally, for comparative purposes, we have normalised all fluxes to the maximum flux capacity of

glucose in the entire model. This point of reference, although entirely arbitrary, enables all fluxes to display comparatively the behaviours of interest.

The reactions included in each of the cells are outlined in **Table 1**. These were chosen to represent the metabolic pathways suspected to be relevant in the myeloma co-culture system. This is a **preliminary assumption** taken for simplicity and will change in future versions in which models will be guided by genomic data.

Reactions	***BMMCS***	***Plasma Cell***
Glycolysis	✓	✓
Tricarboxylic Acid Cycle	✓	✓
Electron Transport Chain	✓	✓
ROS Detoxification	✓	✓
Malate-Aspartate Shuttle	✓	✓
Urea Cycle	✓	✓
5-ALA/Heme Metabolism	✓	
Glutathione Redox	✓	✓
Methionine Pathway	✓	✓
Purine Synthesis/Interconversion	✓	✓
Pyrimidine Synthesis/Interconversion	✓	✓
Glycine, Serine, Alanine, & Theorine Metabolism	✓	✓
Glutamine Metabolism	✓	✓
Valine, Alanine Metabolism		✓
Bicarbonate Buffering	✓	✓
Serine Derived Sphingolipids		✓
FA beta-oxidation	✓	✓

Table 1: *Table of metabolic pathways included in each cell. The reaction pathways in red are exclusive to each cell.*

Finally, the model's **optimisation** was chosen to be **multi-objective**. Although at present the choice of an **adequate objective is not entirely clear**, we have assumed that the **BMMSC's objectives** are: Heme, Pyruvate, and ATP synthesis, whilst the **myeloma cell's objective** is the so-called "biomass" production. The latter involves amino acids, serine-derived lipids, nucleotides, pyrimidines and ATP synthesis. It is unclear what effects, if any, these choices have on the model's predictions. However, future iterations of the model will see in-depth analyses to establish data-driven objectives and their effects on predictive outcomes.

Results

We firstly investigated the fate of BMMSC derived pyruvate. The model predicts a three-pathway flux distribution parting from pyruvate kinases (**PYK**) (Fig.2 **A**). Here, the largest magnitude flux is directed towards the extracellular space via the MCT1 transporter. The myeloma cell, also via MCT1 transporter, introduces the metabolite to its cytoplasm. Here, pyruvate is channelled, in its majority, towards the mitochondria with the sole purpose of TCA cycle support (Fig.2 **B**). A relatively smaller pyruvate flux, from the BMMSC PYKs, is routed towards its lactate dehydrogenases (**LHD**). Seemingly, for oxidation of NADH and thus, sustain the cell's relatively high glycolytic activity. The resultant lactate is then extruded via the membranal MCT4 transporter, where the extracellular space rids lactate out of the microenvironment niche. Finally, the smallest fraction of the glucose-derived pyruvate BMMSC flux is directed towards the cell's own TCA cycle (Fig.2 **A & C**).

The model's flux distribution also indicates that the myeloma cell generates a small glucose-derived pyruvate flux via its pyruvate kinases (**PYK**). Its aim appears to be L-alanine synthesis (Fig.2 **B & D**). Upon MCT1 knockout (**K.O.**), the malignant cell experiences a decrease in pyruvate flux, leading to a limited pyruvate availability. The reduction is also fuelled, in part, due to a prioritisation of the myeloma's glycolytic pathway to gennerate glucose-6-phosphate (**g6p**) and glyceraldehyde 3-phosphate (**g3p**) for nucleotide and L-serine synthesis. Concomitantly, the BMMSC redirects the once membranal MCT1 pyruvate flux, towards its catabolism into lactate causing an increase in MCT4 flux. Interestingly, the

myeloma cell does not redirect or use its MCT4 transporter. We suspect that perhaps, this is an artefact of the objective's choice and should be investigated further.

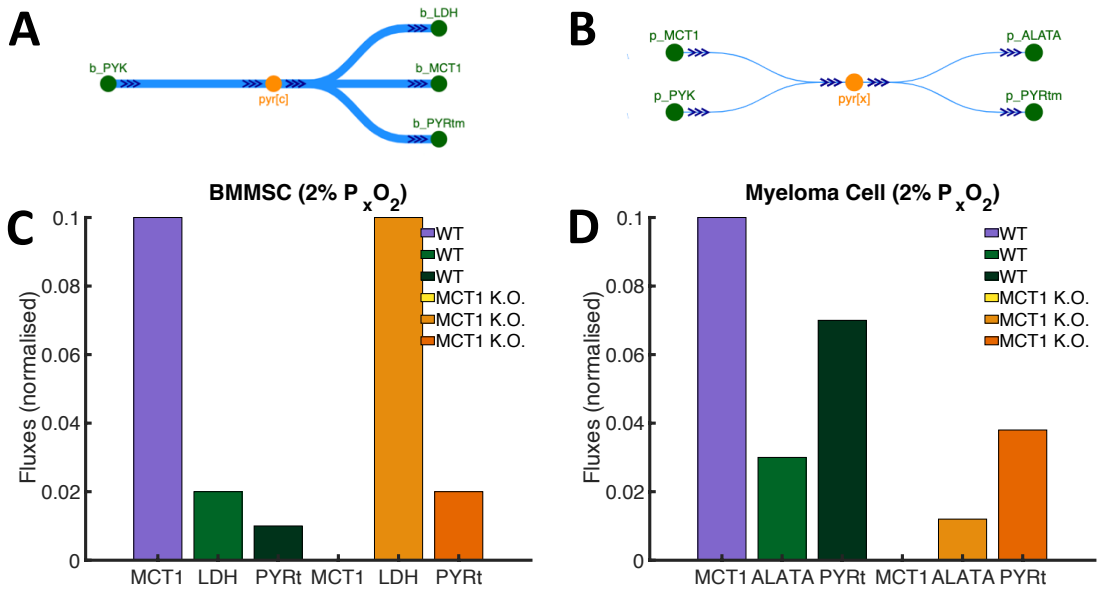

Fig. 2: **A & B.** *Flux schematic depicting the fate of BMMSC glucose-derived pyruvate. After its synthesis by the PYKs, the flux undergoes a three-fold "pitchfork bifurcation", towards the MCT1, LDH, and TCA cycle. The flux from the BMMSC's MCT1 is imported by the myeloma cell, also via MCT1, and directed towards its TCA cycle.* **C.** *Bar graph displaying the BMMSC's pyruvate flux distribution. A large proportion of glucose-derived pyruvate is extruded via the MCT1 whilst a smaller fraction is used to sustain low oxygen glycolysis and the TCA cycle. Upon MCT1 K.O. the flux is redirected towards LDH, where the cell catabolises the metabolite into lactate and then extrudes it via MCT4.* **D.** *Myeloma cell pyruvate flux distribution. The majority of the pyruvate flux is channelled onto the mitochondria to support TCA cycle. A smaller proportion is used to synthesise L-alanine. Upon MCT1 K.O. pyruvate kinases cannot overtake previous pyruvate input, and thus the respective fluxes significantly diminish.*

As mentioned above, the myeloma cell's glycolytic pathway is highly upregulated. Although this is usually a hallmark of cells exposed to hypoxic environments, the resultant flux distribution indicates that in our model, this is almost exclusively to support the production of g6p. Its purpose is to support the pentose-phosphate pathway's production of ribose-5-phosphate, a precursor to 5-phosphoribosyl-1-pyrophosphate via the phosphoribosyl-pyrophosphate synthetase (**PRPPS**) for de-novo nucleotide synthesis. Thus, in the model, the high glycolytic activity of the myeloma cell is not necessarily to oxidise NADH in order to produce glycolysis-derived ATP (Fig. 3**A**). At the same time the glycolytic pathway, and with aid from the pentose-phosphate pathway, produces relatively high amounts of g3p destined for L-serine synthesis via the phosphoserine phosphatase (**PSP**) (Fig. 3**A**). MCT1 disruption drastically reduces the biomass synthesis output of the myeloma cell. An evident fact, as a lack of TCA cycle support, is reflected in a significant decrease in PRPPS and PSP fluxes due to the lack of available ATP. This is, of course, the cell's primary objective (i.e. produce large quantities of biomass). The model's prediction, however, reflects the importance of the glycolytic pathway to sustain proliferation and a total breakdown upon disruption of MCT1 flux (Fig. 3**A**).

Perhaps one of the most significant outcomes of our model concerns the fate of the pyruvate in the myeloma cell once it has been transported to the mitochondrion. Upon its entry, pyruvate is directed, in its majority, towards the pyruvate carboxylase (**PC**), and a smaller fraction is destined towards pyruvate dehydrogenase (**PDH**) (Fig. 3**B**). Several studies suggest that under hypoxia the hypoxia-inducible factor (**HIF**) is responsible for activating pyruvate dehydrogenase kinases (**PDK**), whose activity inhibits PDH to prevent an increase in reactive oxygen species (**ROS**) and thus, prevent cellular damage. To account for the loss of PDH, and as an approximation, we have included beta-oxidation of palmitate - whose task is producing mitochondrial acetyl-CoA. The fluxes related to this pathway seem to have a relatively large impact on the model's TCA cycle. Note that we have allowed the cell to uptake as much palmitate as needed. Disrupting MCT1 activity, causes the cell to undergo a

further increase in palmitate uptake. This is, we suspect, to produce even more acetyl-CoA and sustain the demand for ATP synthesis for biomass production. However, this is seemingly not enough to overcompensate for the loss of incoming pyruvate as the availability of oxygen limits the electron transport chain (**ETC**). In future versions of the model, we will modify the uptake of fatty acids (**FA**) as more experiments reveal the primary role of fatty acids in the co-culture set-up. Taken together, these results are reflected in a decrease of citrate synthesis (Fig.3 **C**).

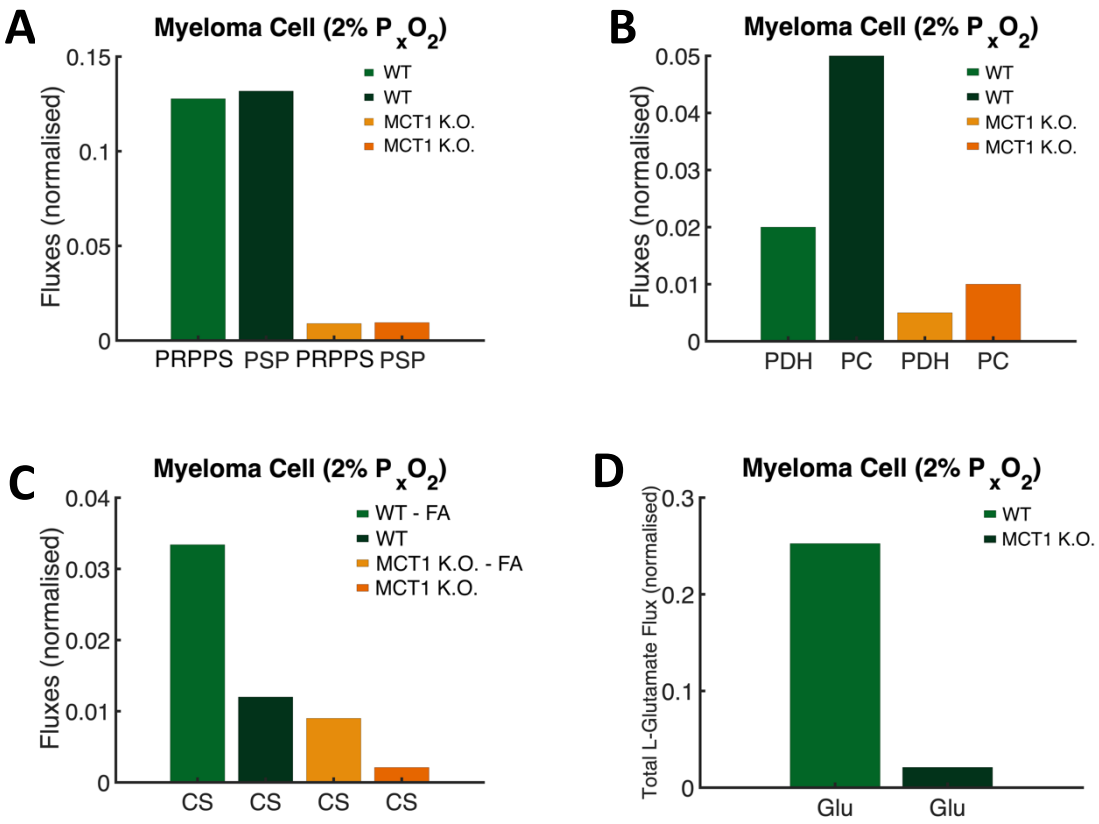

Fig. 3: A. *Although ATP synthesis is crucial via the glycolytic pathway under hypoxia, the model myeloma cell's main purpose is de-novo nucleotide and serine production via the phospho-pentose pathway and the phosphoserine phosphatase, respectively. Upon MCT1 disruption the cell undergoes remodelling of the pathway to sustain ATP production, causing a decrease in these fluxes.* ***B.*** *Once pyruvate is transported towards the mitochondrion, its flux is prioritised towards the pyruvate carboxylases (PC), as opposed to the pyruvate dehydrogenases (PDH). This is in accordance with observations of cells under hypoxia, which see the hypoxia inducible factor HIF activate pyruvate dehydrogenase kinases inhibiting PDH. The necessary acetyl-CoA for TCA cycle activity, in our model, seems to be supplied via fatty acid-beta oxidation. As the glycolytic pathway is unable to overcompensate for the loss of pyruvate, under MCT1 disruption, these fluxes undergo a severe decrease.* ***C.*** *Distinct simulations where the citrate synthases are supplied with FA beta-oxidation-derived acetyl-CoA, under MCT1 knockout and wild type.* ***D.*** *MCT1 disruption effect on the aggregate of glutamate fluxes in the myeloma cell.*

At the same time, in the myeloma's TCA cycle, the oxaloacetate produced by the PC is used to support the aspartate transaminase synthesis of L-aspartate. The majority is exchanged for cytosolic L-glutamate by the electrogenic aspartate/glutamate exchanger (encoded by the Slc25a12/13 gene). This, in turn, serves as a critical step of the malate-aspartate shuttle's activity to oxidise NADH produced by the high glycolytic rates in the myeloma cell. We suspect that, in our model, this is enough to prevent the need for MCT4 activity. Finally, the L-malate transported into the mitochondrion by the L-malate/α-ketoglutarate antiporter is up-taken by the malate dehydrogenase (**MDH**) at the theoretical last step of the TCA cycle. This increases its activity whilst providing a faster rate of mitochondrial reduction of NAD^+, which contributes to the rate at which the ATP is synthesised. Here, the isocitrate dehydrogenase, responsible for metabolising isocitrate into α-ketoglutarate, sees its flux redirected towards the malate-aspartate shuttle to support the demanding oxidation of NADH. This, the model predicts, occurs at the expense of reducing the succinyl-CoA and succinate fluxes of the TCA cycle. Under MCT1 disruption, the rate of cytosolic and mitochondrial NAD^+

regeneration is diminished. This has severe consequences for L-glutamate synthesis, which the model's flux distribution seems to unfavour and thus, affecting the cell biomass objective. Presumably, this is directly related to a disruption of the glutamate/aspartate exchanger, a consequence of the relatively lower TCA cycle's activity (Fig. 3 **D**).

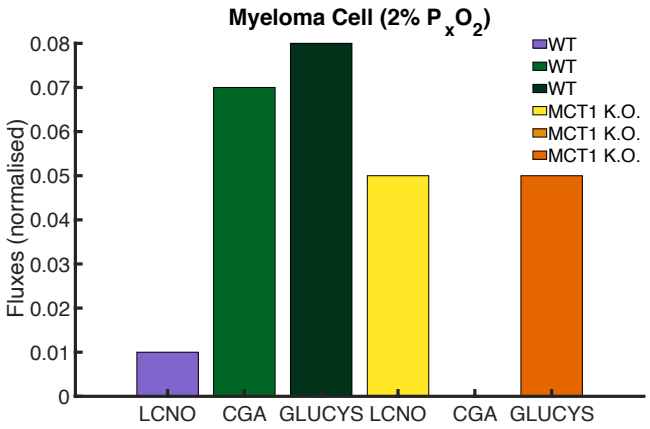

Fig. 4: The flux distribution, under the biomass objective seemingly favours the cystine/glutamate antiporter (CGA) over the synthesis of L-cystine via the L-Cysteine:NAD⁺ Oxidoreductase (LCNO) at the expense of cell import of L-cysteine. In our model the extracellular L-cystine is provided by the BMMSC, which is then used by the myeloma cell to produce gamma-Glutamyl-cysteine, and hence glutathione. Upon MCT1 knockout, the flux distribution sees a shift from L-cystine to L-cysteine to produce L-cystine given a lack of available glutamate.

Our model also predicts that under the hypoxic conditions of the microenvironment niche, the myeloma cell should see an increase in ROS from the ETC's complexes 1 and 3, despite the activity of HIF, whose function should be investigated further in this model. An increase in ROS is critical for the model to sustain a high ATP yield. This is because these increases the flux from superoxide dismutases (**SOD**) and catalases (**CAT**), whose task is to metabolise ROS into oxygen and water. At the same time, the model diversifies the flux of ROS by using glutathione, which is synthesised in the model from L-cystine and L-cysteine along with L-serine derived glycine. This contributes to the high yield of L-serine observed in the model. Interestingly, as the myeloma's objective is to produce "biomass", the glycolytic pathway is already maximising the production of g6p and 3pg which prompts the cell to uptake cysteine from the BMMSC to sustain the synthesis of glutathione and efficiently produce oxygen using ROS. This is enhanced by oxidation of cytosolic NADPH, via the membranal **NOX**, which produces superoxide in the extracellular medium. Extracellular superoxide dismutase catalyses the metabolite into peroxide (and oxygen), which is taken by the cell via peroxiporins (water porins non-selective for peroxide) where glutathione is used to produce water. Upon MCT1 knockout, the production of L-cysteine is decreased, as it is linked to glutamate, which in turn is severely affected. This impairs the system's ETC ATP yield and thus, limiting the cells ability to produce biomass.

In summary, our model yields three important preliminary predictions:

a) Pyruvate is up taken via MCT1 and its critical to support the myeloma's TCA cycle.
b) Glutamate/Glutamine metabolism is at the centre of the metabolism of the malignant cell, and MCT1 knockdown has detrimental effects on its survival.
c) Glutathione synthesis and ROS production are also critical for malignant cell survival.
d) Of particular importance is pH, whose regulation was achieved through the addition of a bicarbonate buffer to balance proton fluxes ($\mathbf{H^+}$). Although its addition is neither intuitive nor immediately apparent, its physiological role is predicted by our preliminary model to be critical in multicellular metabolic modelling and will be included in all future versions as a modelling requirement.

Our objective thus is to refine the model using ^{13}C-Metabolic Flux Analysis to achieve not only qualitative predictions but also quantitative. In this way, we will seek to build a dynamical representation of the same model, where its kinetic parameters will be deducted from the chosen flux distribution resultant from the optimal hyper-cone subset of the multi-objective optimisation space of the constraint-based model (FBA).

To achieve this, we will implement novel algorithms (e.g. Competitive Gradient Descent). To ascertain the resultant flux distribution, the last step will require the generation of an iterative scheme for random sampling of flux hyper-cone; we will use Montecarlo Markov-chain methods like hit and run or Metropolis-Hastings. In this way, a mapping will be formulated, from the CBM solution space to the dynamical model parameter space. Following this, **a parametrised kinetically feasible solution to the dynamical system** will be determined - **based on the experimental data.** The resultant dynamical model will serve to recover temporal transition behaviours in order to investigate the transition from MGUS and MM, where a biological marker will be identified to find a predictor for clinical screening.